

The Impact of Confinement on the Dynamics and H-bonding Pattern in Low-Molecular Weight Poly(propylene glycols)

Agnieszka Talik^{†‡*}, Magdalena Tarnacka^{†‡*}, Monika Geppert-Rybczyńska[§], Barbara Hachuła^{§*}, Kamil Kaminski^{†‡*}, Marian Paluch^{†‡}

[†] Institute of Physics, University of Silesia in Katowice, 75 Pulku Piechoty 1, 41-500 Chorzow, Poland

[‡] Silesian Center of Education and Interdisciplinary Research, University of Silesia in Katowice, 75 Pulku Piechoty 1A, 41-500 Chorzow, Poland

[§] Institute of Chemistry, University of Silesia in Katowice, Szkolna 9, 40-006 Katowice, Poland

* Corresponding authors: *(AT) e-mail: agnieszka.talik@smcebi.edu.pl; (BH) email: barbara.hachula@us.edu.pl; (MT) email: magdalena.tarnacka@smcebi.edu.pl

EXPERIMENTAL SECTION

Materials

Native silica membranes were prepared as presented in Ref.¹ by electrochemical etching of highly doped p-type <100> oriented silicon wafers with resistivity $\leq 0.005 \Omega \text{ cm}$ and thermal oxidation at 1100 K. A mixture of Hydrofluoric acid and Ethanol in the ratio 1:1 was used as an electrolyte. Densities of $j = 20 \text{ mA cm}^{-2}$ were applied to obtain pore diameters of $d = 4 \text{ nm}$ with a porosity of 9-7%. Thickness of used membranes is about $100 \pm 5 \mu\text{m}$. Before filling the templates, they were annealed in high vacuum (10^{-5} mbar) at 470 K for 24 h to remove any volatile impurities.

Silanized SiO₂ membranes were prepared using a mixture of methoxytrimethylsilane (TMMOS, with purity 96+% purchased from Acros Organics) and hexane solvent in the ratio of 1:1 and then annealed at 323 K for 48 h. By treating the membrane with TMMOS, the silanol groups

Qwere replaced with trimethylsilyl groups, and the surface became more hydrophobic². FTIR investigations allow estimating the degree of silanization to be around 95%.

The nanoporous alumina oxide membranes used in this study were supplied from InRedox and composed of uniaxial channels (open from both side) with well- defined pore diameter, $d \sim 18 \pm 2$ nm, thickness $\sim 50 \pm 2$ μm and porosity $\sim 12 \pm 2$ %. Details concerning pore density, distribution, etc. can be found at the Webpage of the producer³. Additionally, dielectric and FTIR spectra as well as DSC thermograms collected for empty native and silanized silica pores of $d = 4$ nm are presented in **Figure S1**.

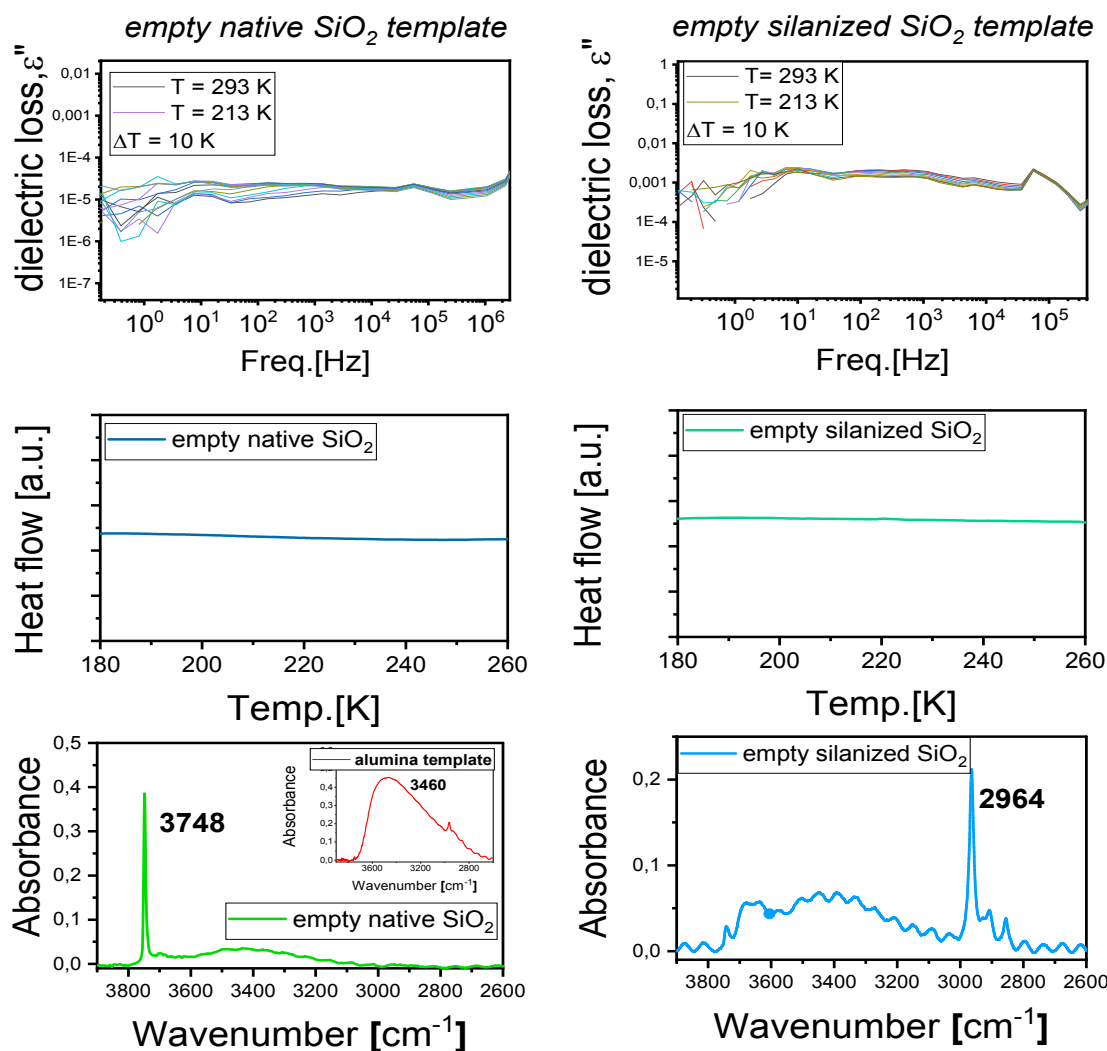


Figure S1. The Spectra of templates before filling obtained from BDS, DSC and FTIR (membranes in the $3900\text{--}2600$ cm^{-1} spectral range) measurements for native and

silanized silica pores ($d=4\text{nm}$). As inset, infrared spectra of the alumina membranes in the $3900\text{--}2600\text{ cm}^{-1}$ spectral range.

1. Methods

2.1. N_2 adsorption/desorption isotherms.

The porosity and pore diameter of SiO_2 membranes of $d=4\text{nm}$ have been determined basing on the low temperature nitrogen adsorption/desorption isotherms measured at 77K by using automatic ASAP 2020 sorption analyzer (Micromeritics Instrument Corp., USA). Prior to the measurement, the established amount (0.18g) of SiO_2 ($d=4\text{ nm}$) support was outgassed ($2\mu\text{mHg}$) at 453 K for 48 h under vacuum in the degas port of the sorption analyzer. The obtained adsorption/desorption isotherms were used to evaluate the structure of the studied material. Data analysis was assessed by means of MicroActive software (Micromeritics). The calculations of the pore size distribution (PSD), and the average BJH desorption pore diameter ($D_{\text{av,des}}$) and the maximum pore diameter ($D_{\text{mo,des}}$) were obtained from the desorption branches of the nitrogen isotherm by means of the Barrett–Joyner–Halenda (BJH) procedure for cylinder pores with Halsey–Faas correction without smooth differentials⁴. The experimental nitrogen adsorption/desorption isotherms and pore-size distribution (PSD) function calculated from desorption branch of isotherm for investigated sample are illustrated in **Figure S2 (a)**. The pore size distribution (PSD) curve for SiO_2 of $d=4\text{ nm}$ was estimated from the desorption branch of nitrogen isotherm using the Barrett–Joyner–Halenda (BJH) model with cylindrical pores (**Figure S2 (b)**). The PSD plot for the investigated material shows relatively narrow pore sizes distribution suggesting that porous structure is fairly uniform; the pores diameter is about $D_{\text{av,des}} \sim 4.27\text{ nm}$, $D_{\text{mo,des}} \sim 4.50$. For characterization of SiO_2 nanopores scanning electron microscopy (SEM) measurements were taken from Ref.⁵, see **Figure S2 (c)**.

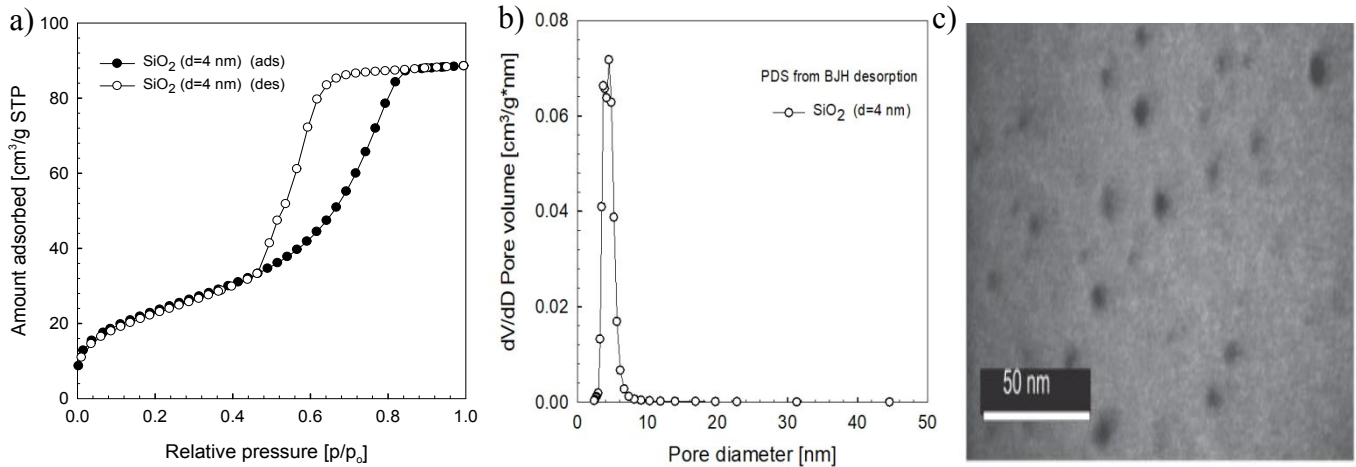


Figure S2. (a) Nitrogen adsorption/desorption isotherms for SiO_2 material ($d = 4 \text{ nm}$); (b) Pore size distribution (PSD) for SiO_2 ($d = 4 \text{ nm}$) calculated from desorption branches of isotherm ; (c) Scanning electron microscope (SEM) images for SiO_2 of $d = 4\text{nm}$ taken from Ref.⁵.

RESULTS

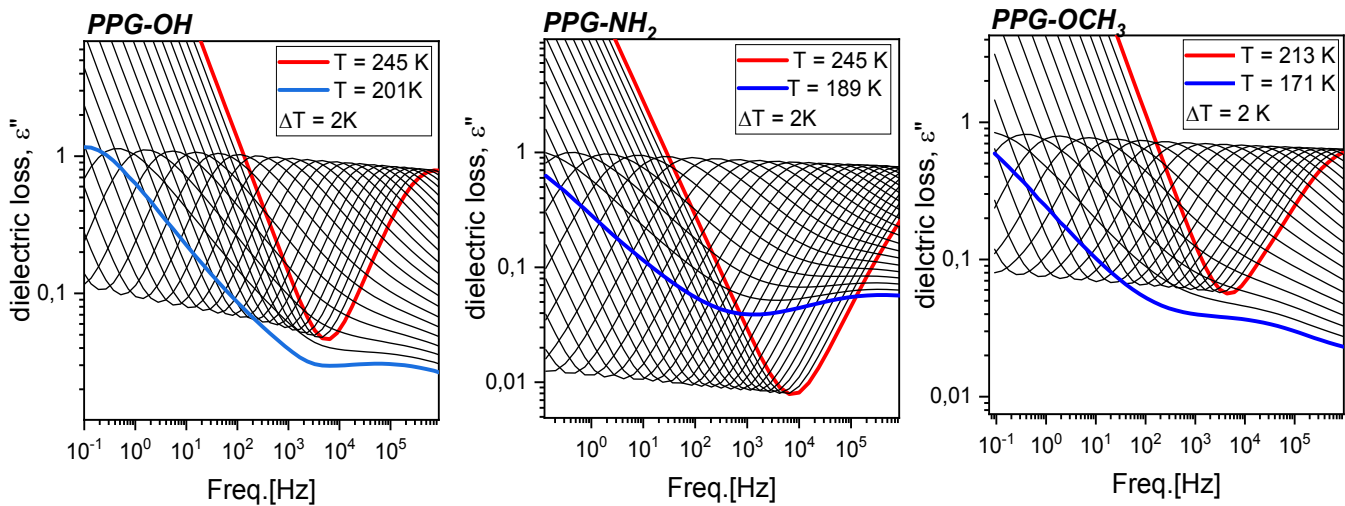


Figure S3. Dielectric loss spectra for bulk PPG's taken from Ref.6

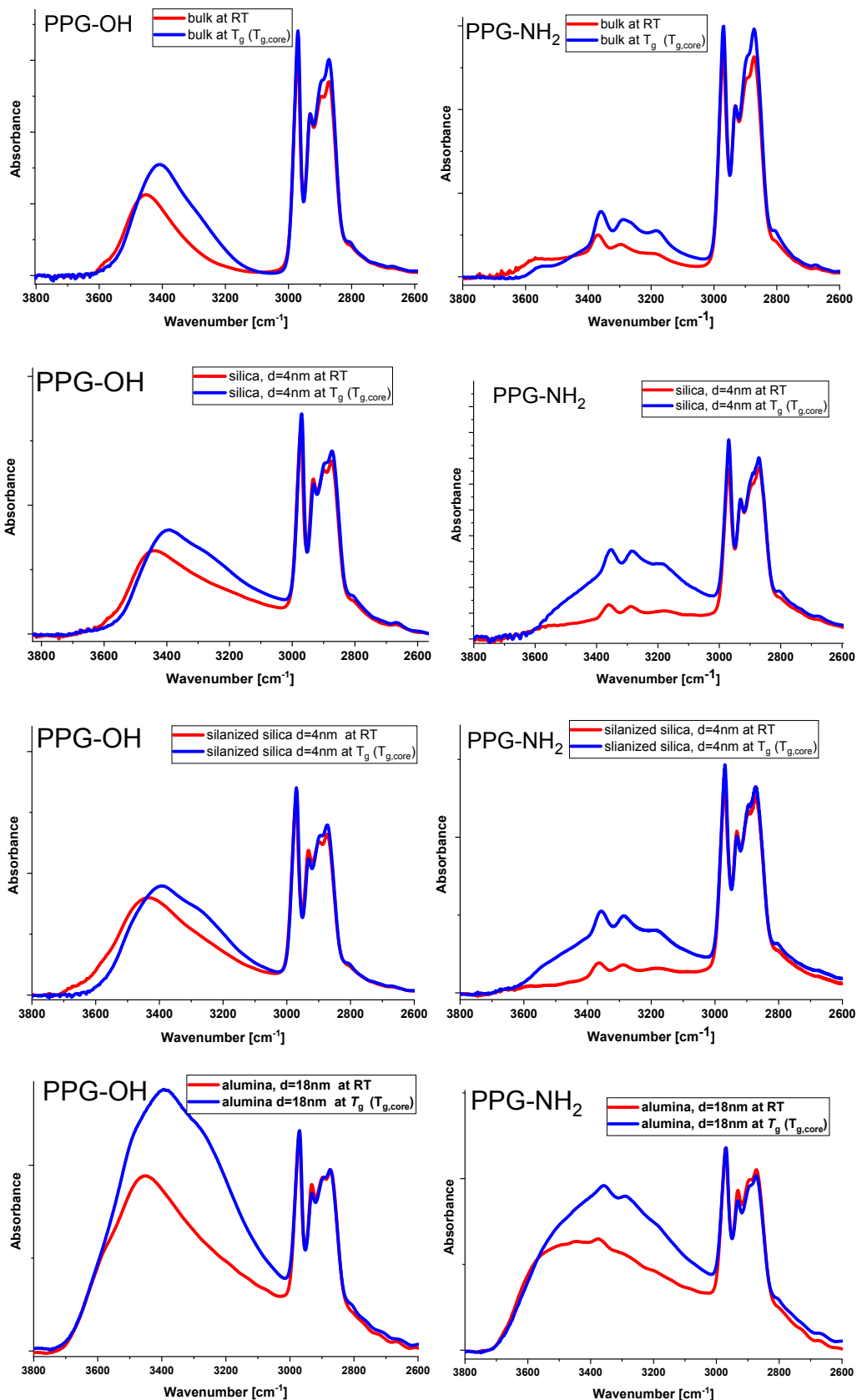


Figure S4. FTIR spectra of bulk and confined PPGs samples within the native silica, silanized silica and alumina pores recorded in the frequency range of 3800-2600 cm⁻¹ measured at room

temperature (red) and the glass transition temperature (blue). The spectra were normalized to the C-H absorption peak at around 2970 cm^{-1} .

The shift towards lower wavenumbers and the corresponding growth of integral intensity of the ν_{X-H} bands is related to the weakening of the X–H bonds, due to an increase of the hydrogen-bond strength, and to the increase of the population of H-bonded aggregates of PPGs molecules, respectively. At T_g , the ν_{X-H} peaks are located at 3407 and 3360, 3289, 3184 cm^{-1} for PPG-OH and PPG-NH₂, respectively ($\Delta\nu = 46\text{ cm}^{-1}$ for PPG-OH; $\Delta\nu = 9, 9, 17\text{ cm}^{-1}$ for PPG-NH₂) (see **Figure S4**). Also, the half-bandwidths of the ν_{X-H} bands are influenced by the effect of temperature i.e. this spectral parameter increases with temperature drop. Therefore, at lower temperature the larger heterogeneity among the hydrogen-bonded moieties of the bulk samples exists.

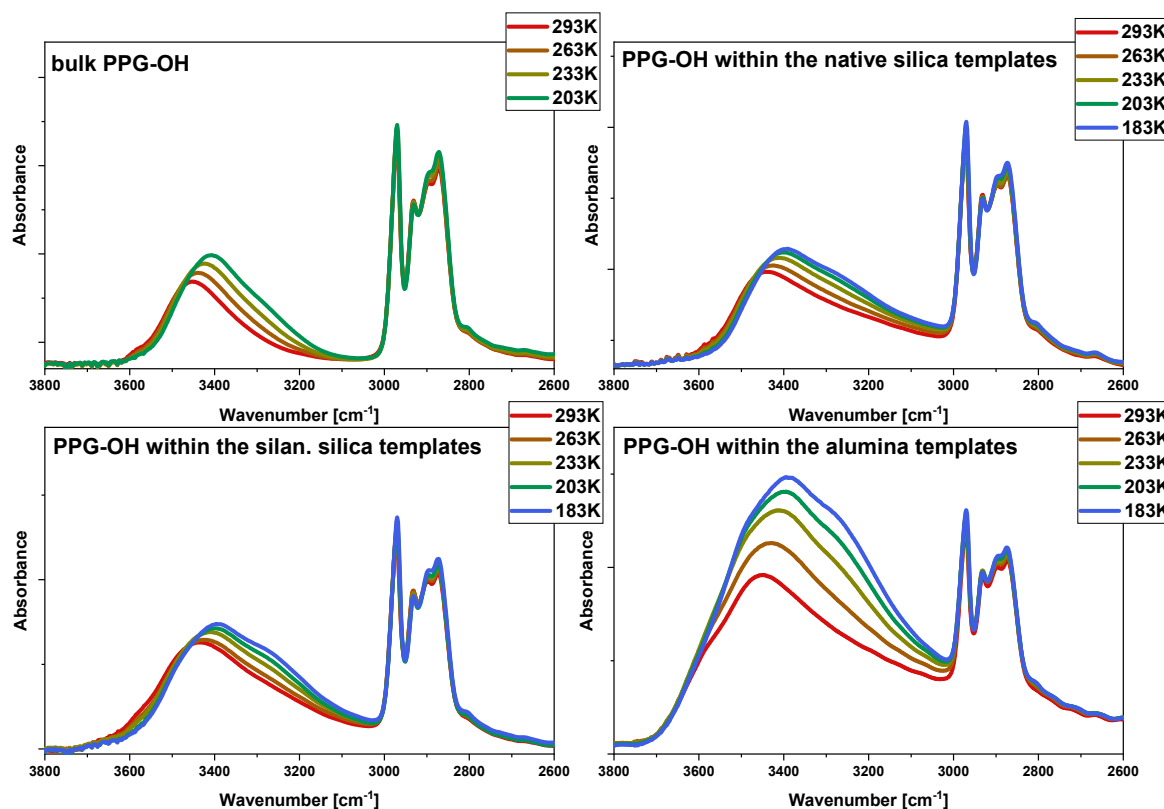


Figure S5. FTIR spectra of bulk and confined PPG-OH in the spectral region of 2600-3800

cm^{-1} in the selected temperatures (bulk: 293K, 263K, 233K, 203K; confined: 293K, 263K, 233K, 203K, 183K).

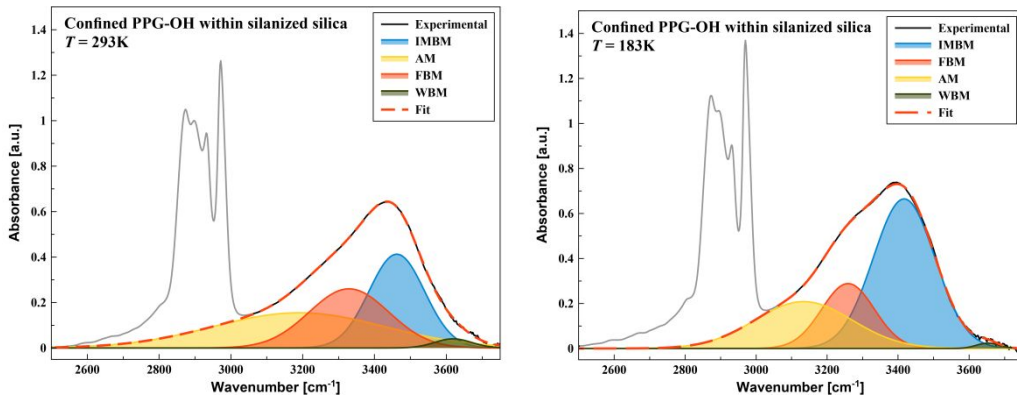


Figure S6. Decomposition of the ν_{OH} band of confined PPG-OH within silanized silica templates in the frequency range of 2500 and 3750 cm^{-1} in the temperatures of 293K and 183K.

T [K]	$\nu_{\text{OH}}^{\text{AM}}$ [cm^{-1}]	$I_{\text{OH}}^{\text{AM}}$ [a.u.]	$\nu_{\text{OH}}^{\text{FBM}}$ [cm^{-1}]	$I_{\text{OH}}^{\text{FBM}}$ [a.u.]	$\nu_{\text{OH}}^{\text{IMBM}}$ [cm^{-1}]	$I_{\text{OH}}^{\text{IMBM}}$ [a.u.]	$\nu_{\text{OH}}^{\text{WBM}}$ [cm^{-1}]	$I_{\text{OH}}^{\text{WBM}}$ [a.u.]
bulk PPG-OH								
293			3363,77	46,49	3459,14	50,69	3585,45	0,56
263			3350,51	57,22	3450,78	55,09	3583,42	0,34
233			3344,03	71,79	3443,12	55,89	3583,93	0,36
203			3335,03	89,87	3432,95	54,55	3589,09	0,39
confined PPG-OH within native silica templates								
293	3194,52	137,36	3393,04	85,15	3463,29	36,46	3606,62	1,98
263	3146,29	115,89	3362,64	105,14	3454,77	52,59	3618,46	3,58
233	3111,9	111,65	3333,84	117,21	3445,17	69,93	3619,08	3,22
203	3073,83	178,24	3318,22	119,78	3433,69	66,33	3648,67	2,59
183	3073,43	217,24	3305,97	112,44	3427,59	69,83	3656,03	1,31
confined PPG-OH within silanized silica templates								
293	3189,76	95,72	3328,95	72,44	3462,12	79,98	3618,88	5,21
263	3171,29	108,80	3328,18	87,59	3454,22	68,89	3616,85	2,89
233	3127,54	63,83	3282,16	64,51	3437,59	123,67	3640,53	4,59
203	3127,67	60,00	3265,17	57,09	3423,13	139,07	3647,78	1,75
183	3133,73	71,29	3258,94	53,59	3416,96	144,73	3652,55	1,89
confined PPG-OH within alumina templates								
293	3197,97	212,18	3361,35	84,00	3482,48	98,60	3603,24	17,83
263	3167,53	235,03	3339,15	125,19	3473,58	126,59	3594,87	20,01
233	3143,43	238,01	3319,33	167,97	3463,96	151,11	3581,22	30,19
203	3095,95	196,22	3291,44	183,07	3453,42	205,89	3578,38	33,19

183	3026,01	154,14	3293,60	278,29	3460,08	200,11	3586,75	23,87
-----	---------	--------	---------	--------	---------	--------	---------	-------

Table S1. Best-fit parameters (the peak position ν and the peak area I) of the OH stretching band for bulk and confined PPG-OH.

T [K]	AM [%]	FBM [%]	IMBM [%]	WBM [%]
<i>bulk PPG-OH</i>				
293		47,56	51,86	0,58
263		50,79	48,90	0,31
233		56,07	43,65	0,28
203		62,06	37,67	0,27
<i>confined PPG-OH within native silica templates</i>				
293	52,64	32,63	13,97	0,76
263	41,81	37,93	18,97	1,29
233	36,97	38,81	23,15	1,07
203	48,58	32,64	18,07	0,71
183	54,20	28,05	17,42	0,33
<i>confined PPG-OH within silanized silica templates</i>				
293	37,78	28,59	31,57	2,06
263	40,57	32,66	25,69	1,08
233	24,87	25,14	48,19	1,80
203	23,26	22,13	53,92	0,68
183	26,26	19,74	53,31	0,69
<i>confined PPG-OH within alumina templates</i>				
293	51,42	20,36	23,89	4,33

263	46,37	24,70	24,98	3,95
233	40,53	28,60	25,73	5,14
203	31,73	29,60	33,29	5,38
183	23,48	42,40	30,48	3,64

Table S2. Ratio of the ν_{OH} peak area obtained from spectral fittings for bulk and confined PPG-OH.

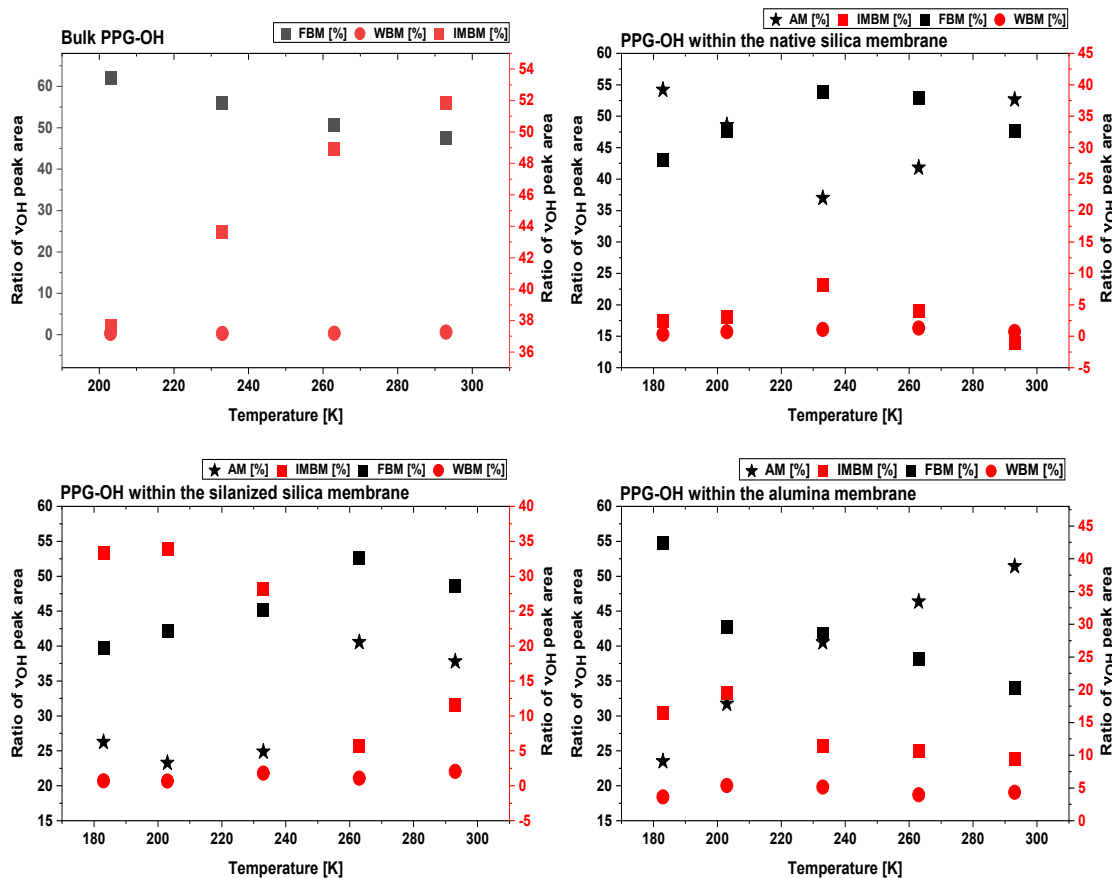


Figure S7. The temperature evolution of peak areas obtained from the -OH band of bulk and confined PPG-OH by the superposition of the few Gaussian functions assigned to vibration of this moiety in the following fractions of oligomers AM, IMBM, FBM, WBM.

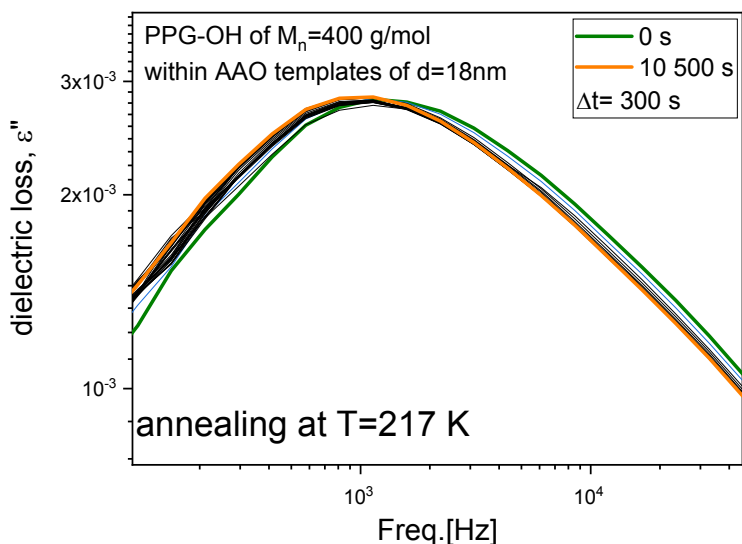


Figure S8. Dielectric loss spectra collected upon annealing of confined samples at $T = 217$ K measured for PPG-OH of $M_n = 400$ g/mol confined in AAO templates of $d = 18$ nm taken from Ref.6.

References:

1. Kipnusu, W. K.; Kossack, W.; Iacob, C.; Jasiurkowska, M.; Sangoro, J.R.; Kremer, F. Molecular Order and Dynamics of Tris(2-ethylhexyl)phosphate Confined in Uni-Directional Nanopores. *Z. Phys. Chem.* **2012**, *226*, 797–805.
2. Iacob, C.; Sangoro, J.R.; Papadopoulos, P.; Schubert, T.; Naumov, S.; Valiullin, R.; Karger, J.; Kremer, F. Charge Transport and Diffusion of Ionic Liquids in Nanoporous Silica Membranes. *Phys. Chem. Chem. Phys.* **2010**, *12*, 13798–13803.
3. <https://www.inredox.com>
4. Barrett, E.P.; Joyner, L.G.; Halenda, P.P. The determination of pore volume and area distributions in porous substances. I. Computations from nitrogen isotherms. *J. Am. Chem. Soc.* **1951**, *73*, 373–80.
5. Iacob, C.; Sangoro, J.R.; Kipnusu, W.K.; Valiullin, R.; Kärger, J.; Kremer, F. Enhanced charge transport in nano-confined ionic liquids. *Soft Matter*, **2012**, *8*(2), 289–293.
6. Tarnacka, M.; Talik, A.; Kamińska, E.; Geppert-Rybczyńska, M.; Kaminski, K.; Paluch, M. The Impact of Molecular Weight on the Behavior of Poly(propylene glycols) Derivatives Confined within Alumina Templates. *Macromolecules* **2019**, *52* (9), 3516–3529.